Hindawi Publishing Corporation
International Journal of Antennas and Propagation
Volume 2015, Article ID 401210, 7 pages
http://dx.doi.org/10.1155/2015/401210

Research Article

Full-Wave Analysis of Stable Cross Fractal Frequency Selective Surfaces Using an Iterative Procedure Based on Wave Concept

V. P. Silva Neto,[1,2] M. J. Duarte,[1] and A. G. D'Assunção[2]

[1]*Federal Rural University of the Semiarid Region, DEE, RN 233, km 01, 59780-000 Caraúbas, RN, Brazil*
[2]*Federal University of Rio Grande do Norte, UFRN-CT-DCO, P.O. Box 1655, 59078-970 Natal, RN, Brazil*

Correspondence should be addressed to V. P. Silva Neto; valdemir.neto@ufersa.edu.br

Received 25 March 2015; Revised 25 June 2015; Accepted 1 July 2015

Academic Editor: Xianming Qing

This work presents a full-wave analysis of stable frequency selective surfaces (FSSs) composed of periodic arrays of cross fractal patch elements. The shapes of these patch elements are defined conforming to a fractal concept, where the generator fractal geometry is successively subdivided into parts which are smaller copies of the previous ones (defined as fractal levels). The main objective of this work is to investigate the performance of FSSs with cross fractal patch element geometries including their frequency response and stability in relation to both the angle of incidence and polarization of the plane wave. The frequency response of FSS structures is obtained using the wave concept iterative procedure (WCIP). This method is based on a wave concept formulation and the boundary conditions for the FSS structure. Prototypes were manufactured and measured to verify the WCIP model accuracy. A good agreement between WCIP and measured results was observed for the proposed cross fractal FSSs. In addition, these FSSs exhibited good angular stability.

1. Introduction

Frequency selective surfaces (FSSs) are being designed for many applications in modern communication systems. Typically, they are used as spatial filters of electromagnetic waves and are composed of two-dimensional periodic arrays of metallic patch or aperture elements, behaving like band-stop or band-pass filters, respectively [1–4]. Therefore, FSSs are used to reflect or transmit electromagnetic waves according to their array geometry, resonant element type and shape, and other structural parameters. Therefore, different FSS geometries may be used depending upon the desired frequency response.

Furthermore, each FSS element resonates and dispenses energy around its resonance frequency, when there are incident electromagnetic waves. Typically, FSSs with aperture type elements are used to provide band-pass filter response with incident wave transmission at resonant frequencies. Similarly, FSSs with metallic patch type elements are used to provide band-stop filter response with incident wave reflection at resonant frequencies [5, 6].

The frequency response of a periodic FSS geometry depends on the element shape and type, substrate parameters, and array type and periodicity. Therefore, FSSs are used in many microwave applications such as radomes, subreflectors, antenna systems, absorbers, and ovens.

Recently, several papers were devoted to study improvements on the performance of FSS geometries, such as polarization independence, angular stability, and array element size reduction [7–9]. Particularly, the use of fractal elements in FSS designs has proved to be an effective method to miniaturize FSS elements and to obtain good angular stability (in relation to oblique incidence of the plane wave).

This work presents a full-wave analysis of periodic FSS structures with cross fractal patch elements. This element shape is based on a combination of circular and cross dipole conductive patches. Prototypes of band-stop filters are designed, fabricated, and measured for comparison purposes.

Moreover, this work aims to investigate the proposed FSS geometry properties, regarding miniaturization, angular stability, and polarization independence. An analysis of the

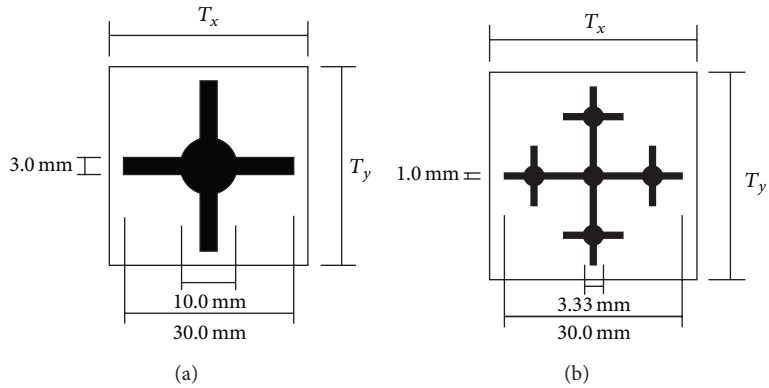

Figure 1: Cross fractal FSS elements: (a) generator and (b) first fractal iteration.

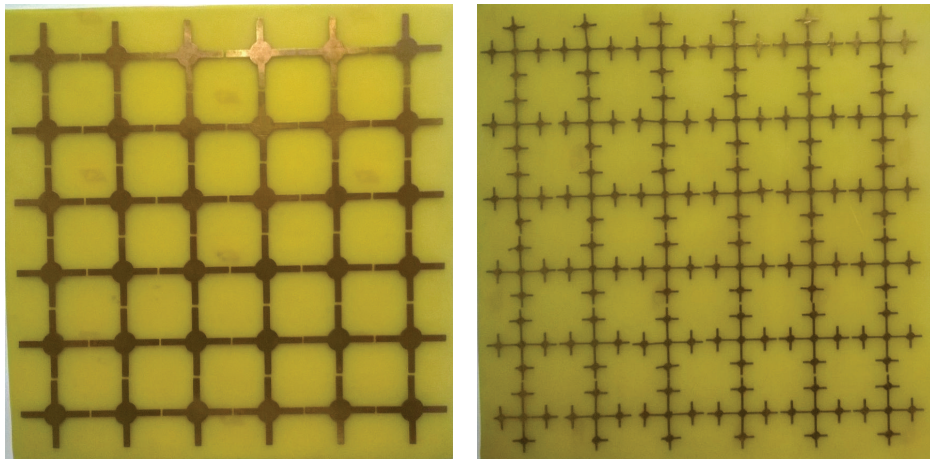

Figure 2: Photographs of FSS prototypes fabricated with cross fractal patch element geometries: (a) generator and (b) first fractal iteration.

array periodicity was carried out to verify its influence on the FSS frequency response.

Theoretical results were obtained using an integral and iterative method based on transversal wave concept (WCIP). The WCIP method solves electromagnetic problems using the concept of incident, reflected, and transmitted waves on a circuit interface. Therefore, this method is suitable to analyze planar microwave circuits [10], patch antennas, and FSSs [11–16]. The WICP method uses FFT to reduce the required computing time and provide both versatility and reliable representation of the circuit structure.

WCIP results for the frequency behavior of the designed FSS were obtained and compared to simulated results by Ansoft HFSS and experimental results, for validation purpose. Measured results were obtained using a vector network analyzer (Agilent Technologies, model N5230A) and two horn antennas. A good agreement between simulated and measured results was verified.

2. FSS Design

The FSS elements used in this work are presented in Figure 1. The generator is based on the combination of a circular patch element, with diameter equal to 10 mm, and a cross dipole element, with length equal to 30 mm and width 3 mm, as shown in Figure 1(a). Figure 1(b) presents the fractal geometry for the first fractal iteration, according to the cross fractal formation rule.

Figure 2 depicts photographs of the fabricated FSS prototypes. The design of FSS structures with cross fractal geometries was developed taking into account the resonant properties of the cross fractal elements. For example, the autosimilarity, provided by the cross fractal element nature, increases the electrical length traversed by the surface current on the patch, resulting in lower resonant frequencies or reduced sizes (if the frequency design requirement is maintained). Therefore, the proposed cross fractal patch geometries can be used to decrease the FSS resonant frequency, to provide multiband behavior, or to reduce the patch element dimensions, and to develop FSS structures with angular stability and independence of polarization.

3. WCIP Theoretical Formulation

The wave concept iterative procedure (WCIP) is an integral and iterative method that consists in separating the FSS

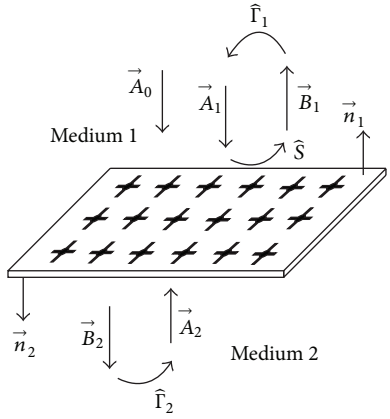

Figure 3: WCIP formulation at the circuit interface.

structure in interfaces with upper and lower homogeneous media as shown in Figure 3. The boundary conditions at the circuit surface are represented by a scattering parameter, $\hat{S}$, defined in the spatial domain. The propagation conditions in the homogeneous media are described by the reflection coefficient operator, $\hat{\Gamma}$, defined in the modal domain.

Basically, the WCIP method is described by two equations that relate the incident ($\vec{A}_i$) and reflected ($\vec{B}_i$) waves at the circuit interface. These equations are given in

$$\begin{aligned} \vec{B}_i &= \hat{S}\vec{A}_i + \vec{A}_0, \\ \vec{A}_i &= \hat{\Gamma}\vec{B}_i, \end{aligned} \tag{1}$$

where $\vec{A}_0$ is a local electromagnetic wave source defined throughout the space domain that focuses on the FSS interface from one of the means. The relationship between the incident and the reflected waves and the independent variables, which are the tangential electric field $\overrightarrow{E}_{Ti}$ and the tangential magnetic field $\vec{H}_{Ti}$, are given by

$$\begin{aligned} \vec{A}_i &= \frac{1}{2\sqrt{Z_{0i}}}\left(\vec{E}_i + Z_{0i}\left(\vec{H}_{Ti}\times\vec{n}\right)\right), \\ \vec{B}_i &= \frac{1}{2\sqrt{Z_{0i}}}\left(\vec{E}_i - Z_{0i}\left(\vec{H}_{Ti}\times\vec{n}\right)\right), \end{aligned} \tag{2}$$

where i indicates medium 1 or 2 at the interface and Z_{0i} is the characteristic impedance of medium i, given by

$$Z_{0i} = \sqrt{\frac{\mu_0}{\varepsilon_0\varepsilon_{ri}}}; \tag{3}$$

μ_0 and ε_0 are the free space permeability and permittivity, respectively, and ε_{ri} is the relative permittivity of medium i.

In the WCIP method, (1) are established in each point at the discontinuity surface, which is divided in pixels. For each pixel a different scattering operator is associated, and this operator will consider the boundary conditions on this particular point of the circuit surface. Different boundary conditions can be considered such as those related to dielectric, metal, source, or load pixel. For the FSS studied in this work, we can identify two different cases for the scattering operator. At metal pixels we use the operator shown in (4) and at dielectric pixels we use the operator shown in (5):

$$\hat{S}_{\text{metal}} = \begin{pmatrix} -1 & 0 \\ 0 & -1 \end{pmatrix}, \tag{4}$$

$$\hat{S}_{\text{dielectric}} = \begin{pmatrix} \dfrac{\eta^2-1}{\eta^2+1} & \dfrac{2\eta}{\eta^2+1} \\ \dfrac{2\eta}{\eta^2+1} & -\dfrac{\eta^2-1}{\eta^2+1} \end{pmatrix}, \tag{5}$$

where $\eta = \sqrt{Z_{01}/Z_{02}}$ and Z_{01} and Z_{02} are the characteristic impedance of media 1 and 2, respectively. The source is modeled as a distributed source defined in the modal domain without changing the scattering parameter.

The reflection coefficient operator, $\hat{\Gamma}$, assigns the propagation boundary conditions on the upper and lower media and takes into account the characteristics of the wave propagation in the medium around the circuit interface. This operator defines the relationships between the incident and reflected waves in the media around the circuit interfaces. In addition, it is defined in the modal domain, because the wave is decomposed into TE_{mn} and TM_{mn} modes, which are taken into account considering the reflection coefficients given by (6) and (7), where $m = 1, 2, 3, \ldots$, and $n = 1, 2, 3, \ldots$, respectively:

$$\hat{\Gamma}^{\text{TE}}_{mn,i} = \frac{1 - Z_{0i}Y^{\text{TE}}_{mn,i}}{1 + Z_{0i}Y^{\text{TE}}_{mn,i}}, \tag{6}$$

$$\hat{\Gamma}^{\text{TM}}_{mn,i} = \frac{1 - Z_{0i}Y^{\text{TM}}_{mn,i}}{1 + Z_{0i}Y^{\text{TM}}_{mn,i}}; \tag{7}$$

Z_{0i} is the characteristic impedance of medium i and $Y^{\text{TE}}_{mn,i}$ and $Y^{\text{TM}}_{mn,i}$ are, respectively, the TE_{mn} and TM_{mn} modes equivalent admittances for medium i. The link between the spatial and modal domains is obtained using the Modal Fourier Transform (FMT). Initially, the waves are described in the spectral domain by the fast Fourier transform (FFT). Then, they are decomposed into waves of TE_{mn} and TM_{mn} modes passing them to the modal domain [14]. This procedure is repeated until convergence is achieved.

4. Results and Discussion

The first step of this work is search the best value for the array periodicity of the FSS geometry for a given frequency band. In this case, a parametric study was performed on the periodicity of FSS. Figures 4(a) and 4(b) show the transmission coefficient as function of frequency, for different values of the FSS array periodicity. We should search for the best value of array periodicity to get a good frequency response for the FSS geometry with the generator elements, shown in Figure 2(a), in the WiMax frequency range.

Taking into account the results shown in Figure 4, we chose those corresponding to an array periodicity, T, equal

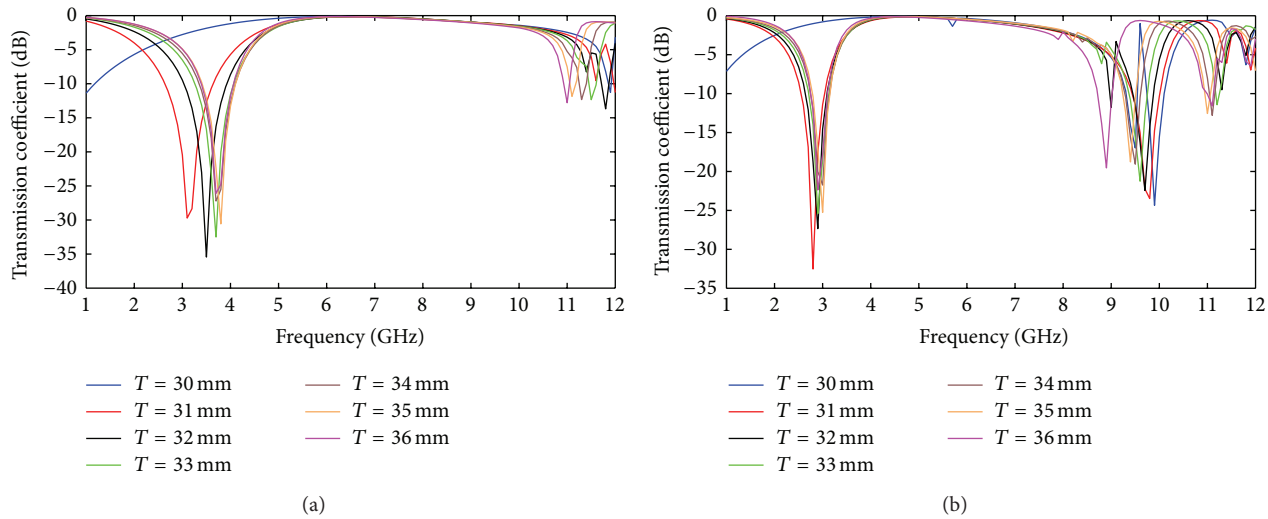

FIGURE 4: Simulation results for the transmission coefficient for different FSS array periodicity values: (a) FSS_1 (generator) and (b) FSS_2 (first fractal iteration).

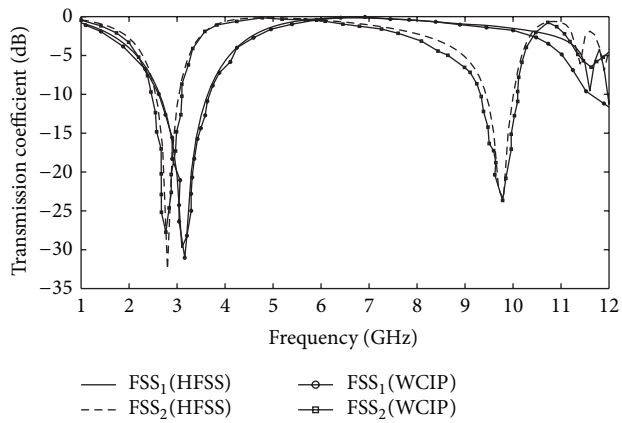

FIGURE 5: Simulated results for the transmission coefficient for FSS with cross fractal patch elements shown in Figure 2.

to 32 mm (FSS_1). In this particular case the FSS presents a good frequency response in the WiMax frequency range, with a resonant frequency equal to 3.2 GHz, a bandwidth (BW) equal to 0.9 GHz, and a transmission coefficient (S_{21}) equal to −29.72 dB.

Figure 5 shows the results for the transmission coefficient for the FSS geometries with cross fractal elements, shown in Figure 2. We confirmed an inversely proportional relationship between the FSS resonant frequencies and the fractal level of the proposed FSS patch elements. The accuracy of the WCIP method was verified by comparing simulated WCIP and HFSS results.

Figure 6 presents simulated (WCIP and HFSS) and measured results for the transmission coefficient of the FSS with generator elements (FSS_1). The WCIP results for the resonant frequency and bandwidth (for a −10 dB reference) are 3.26 GHz and 1.02 GHz, respectively. The measured results are in good agreement with the WCIP simulated ones, presenting a relative error of 1.7% at the resonant frequency. The measured bandwidth (BW) result is 1.03 GHz, presenting a relative error of 0.1% with respect to the WCIP result.

Figure 7 depicts the frequency response of the FSS with cross fractal patch elements (FSS_2). The curve shows that the FSS has a first resonant frequency at 2.73 GHz with an insertion loss equal to −25.68 dB and a bandwidth of 650 MHz. This FSS geometry presents a second resonance at 9.77 GHz with $S_{21} = -24.90$ dB and a bandwidth BW = 910 MHz. We verified that the FSS with cross fractal patch elements (FSS_2) exhibited a compression factor of 15.34%, enabling a FSS patch element size reduction. Also, we verified a dual band behavior in the considered frequency range.

The angular stability and independence of polarization for the proposed FSS structures were investigated by varying the plane wave incidence angle from 0° (normal incidence) to 60°, with a 20° step, as shown in Figures 8 and 9.

Figure 8 shows measured results of the transmission coefficient frequency behavior for the proposed FSS structures: (a) FSS_1 and (b) FSS_2 and TE polarization. Figure 9 shows measured results of the transmission coefficient frequency behavior for the proposed FSS structures: (a) FSS_1 and (b) FSS_2 and TM polarization.

Table 1 exhibits measured values for the proposed FSSs first resonant frequency, f_r, and bandwidth, BW, in order to compare their angular stability and polarization independence performances.

According to measured results, the FSS with cross fractal elements has a good angular stability with respect to the plane wave incidence angle. In addition, the analyzed FSS_1 structure, with generator elements, presented high independence in relation to the polarization plane wave incident, at the first resonance, and a tuning possibility at the second resonance band. However, the analyzed FSS_2 structure, with first fractal iteration elements, presented high independence in relation to the polarization plane wave incident, at the first and second resonance bands.

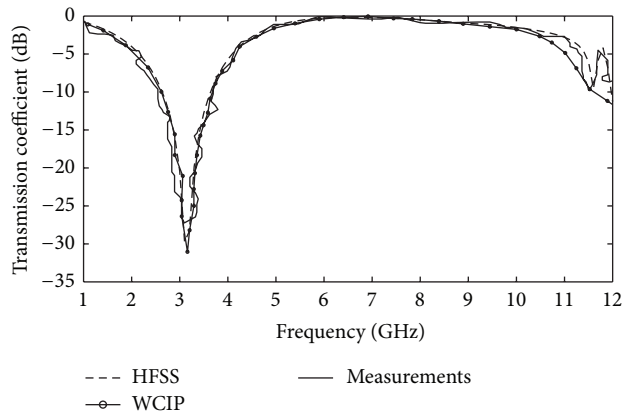

Figure 6: Simulated and measured results of the transmission coefficient for the FSS with cross fractal patch elements (FSS_1).

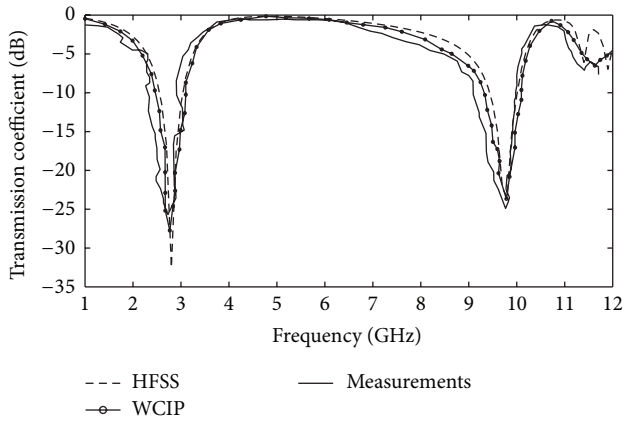

Figure 7: Simulated and measured results of the transmission coefficient for the FSS with cross fractal patch elements (FSS_2).

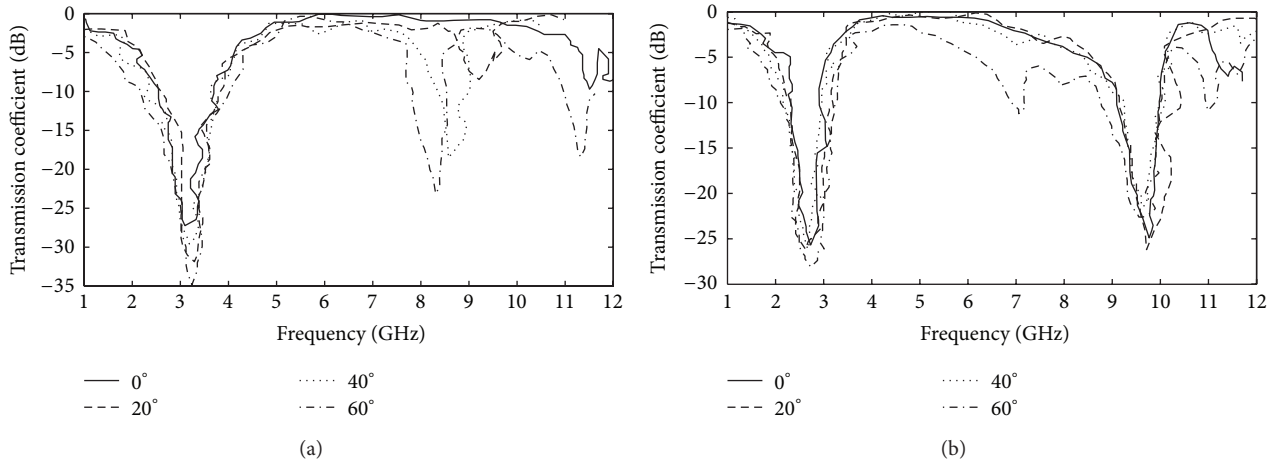

Figure 8: Measured transmission coefficient concerning the plane wave incidence angle and TE polarization for the proposed FSS structures: (a) FSS_1 and (b) FSS_2.

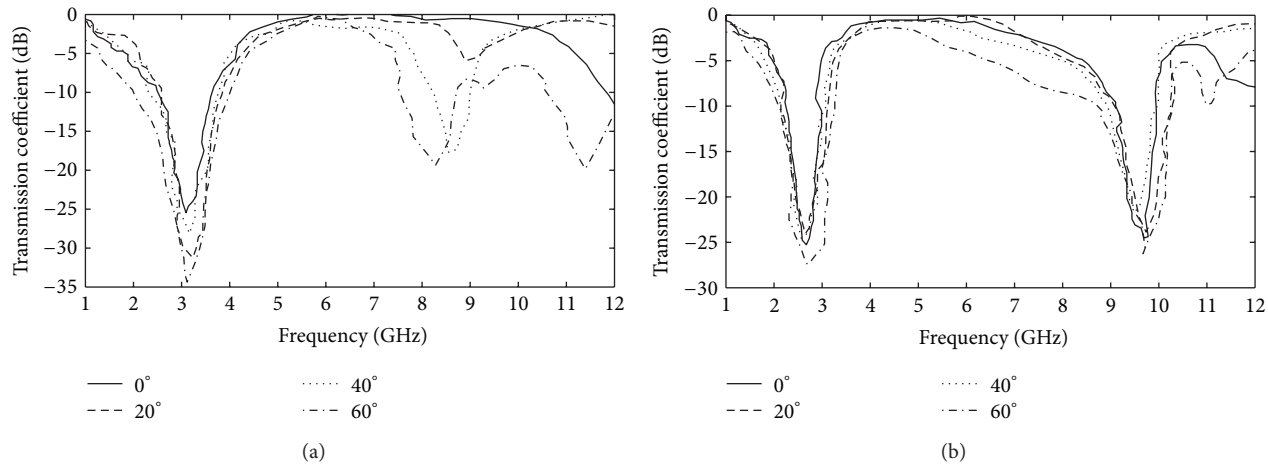

Figure 9: Measured transmission coefficient concerning the plane wave incidence angle and TM polarization for the proposed FSS structures: (a) FSS_1 and (b) FSS_2.

Table 1: Measured results for FSS transmission coefficient frequency behaviors concerning the plane wave incidence angle and TE and TM polarization.

θ	FSS_1				FSS_2			
	TE		TM		TE		TM	
	f_r (GHz)	BW (GHz)	f_r (GHz)	BW (GHz)	f_r (GHz)	BW (GHz)	f_r (GHz)	BW (GHz)
0°	3.26	1.02	3.18	1.02	2.73	0.650	2.70	0.649
20°	3.28	1.25	3.24	1.22	2.69	0.900	2.71	0.953
40°	3.19	1.36	3.17	1.42	2.70	0.960	2.70	0.953
60°	3.24	2.09	3.17	2.11	2.73	1.14	2.72	1.15

5. Conclusions

In this work, we analyzed and designed FSSs with cross fractal frequency selective surfaces. The FSS structures were analyzed by theoretical and experimental investigation. Particularly, the proposed FSS geometries were analyzed through the efficient and accurate WCIP method. Thereafter, HFSS and measured results were obtained for comparison purpose. It was shown that the proposed FSS geometries presented excellent polarization stability, angular stability, and patch element miniaturization. In addition, the FSS design methodology described in this paper was validated by excellent agreement observed between theoretical (WCIP), simulation (HFSS), and measured results.

Conflict of Interests

The authors declare that there is no conflict of interests regarding the publication of this paper.

Acknowledgments

This work was supported by CNPq, under covenant 573939/2008-0 (INCT-CSF) and under contract 552659/2011-8, CAPES, Federal University of Rio Grande do Norte (UFRN), and Federal Rural University of the Semiarid Region (UFERSA).

References

[1] J. I. A. Trindade, P. H. F. Silva, A. L. P. S. Campos, and A. G. D'Assunção, "Analysis of stop-band frequency selective surfaces with Dürer's pentagon pre-fractals patch elements," *IEEE Transactions on Magnetics*, vol. 47, no. 5, pp. 1518–1521, 2011.

[2] B. Sanz-Izquierdo and E. A. Parker, "Dual polarized reconfigurable frequency selective surfaces," *IEEE Transactions on Antennas and Propagation*, vol. 62, no. 2, pp. 764–771, 2014.

[3] J. Romeu and Y. Rahmat-Samii, "Fractal FSS: a novel dual-band frequency selective surface," *IEEE Transactions on Antennas and Propagation*, vol. 48, no. 7, pp. 1097–1105, 2000.

[4] H.-Y. Yang, S.-X. Gong, P.-F. Zhang, F.-T. Zha, and J. Ling, "A novel miniaturized frequency selective surface with excellent center frequency stability," *Microwave and Optical Technology Letters*, vol. 51, no. 10, pp. 2513–2516, 2009.

[5] T. K. Wu, Ed., *Frequency Selective Surface and Grid Array*, Wiley, New York, NY, USA, 1995.

[6] B. A. Munk, *Frequency-Selective Surfaces: Theory and Design*, Wiley, New York, NY, USA, 2000.

[7] A. G. D'Assunção Jr., G. Fontgalland, A. Gomes Neto, and H. Baudrand, "Frequency selective surface filters with polarized band pass/band reject performances," *Microwave and Optical Technology Letters*, vol. 56, no. 2, pp. 483–487, 2014.

[8] P. H. F. Silva, C. L. Nóbrega, M. R. Silva, and A. G. d'Assunção, "Optimal design of frequency selective surfaces with fractal motifs," *IET Microwaves, Antennas & Propagation*, vol. 8, no. 9, pp. 627–631, 2014.

[9] M. R. Silva, A. G. D'Assunção, P. H. Fonseca da Silva, and C. L. Nóbrega, "Stable and compact multiband frequency selective surfaces with Peano pre-fractal configurations," *IET Microwaves, Antennas & Propagation*, vol. 7, pp. 543–551, 2013.

[10] V. P. Silva Neto, *Characterization of microwave printed circuits using WCIP method [M.S. thesis]*, Federal University of Rio Grande do Norte, Natal, Brazil, 2013, (Portuguese).

[11] P. B. C. Medeiros, V. P. Silva Neto, and A. G. D'Assunção, "A compact and stable design of FSS with radial slit circular elements using an iterative method," *Microwave and Optical Technology Letters*, vol. 57, no. 3, pp. 729–733, 2015.

[12] M. Titaouine, A. G. Neto, H. Baudrand, and F. Djahli, "Analysis of frequency selective surface on isotropic/anisotropic layers using WCIP method," *ETRI Journal*, vol. 29, no. 1, pp. 36–44, 2007.

[13] A. Serres, G. K. F. Serres, G. Fontgalland, R. C. S. Freire, and H. Baudrand, "Analysis of multilayer amplifier structure by an efficient iterative technique," *IEEE Transactions on Magnetics*, vol. 50, no. 2, pp. 185–188, 2014.

[14] R. S. N'Gongo and H. Baudrand, "Application of wave concept iterative procedure in planar circuit," *Recent Research Developments in Microwave Theory and Technique*, vol. 1, pp. 187–197, 1999.

[15] G. A. Cavalcante, A. G. D'Assunção Jr., and A. G. D'Assunção, "An iterative full-wave method for designing bandstop frequency selective surfaces on textile substrates," *Microwave and Optical Technology Letters*, vol. 56, no. 2, pp. 383–388, 2014.

[16] M. Titaouine, A. Gomes Neto, H. Baudrand, and F. Djahli, "WCIP method applied to active frequency selective surfaces," *Journal of Microwaves and Optoelectronics*, vol. 6, no. 1, pp. 1–16, 2007.